

**SAND2002-1320**  
Unlimited Release  
Printed May 2002

**Sandia Smart Anti-Islanding Project**  
**Summer 2001**

**Task II**  
**Investigation of the Impact of Single-phase**  
**Induction Machines in Islanded Loads**

**Summary of Results**

Mike Ropp  
South Dakota State University  
Brookings, SD 57007

Russell Bonn and Sigifredo Gonzalez  
Photovoltaic Systems  
Sandia National Laboratories  
P. O. Box 5800  
Albuquerque, NM 87185-0753

Chuck Whitaker  
Endecon Engineering  
San Ramon, CA 94583

**ABSTRACT**

Islanding, the supply of energy to a disconnected portion of the grid, is a phenomenon that could result in personnel hazard, interfere with reclosure, or damage hardware. Considerable effort has been expended on the development of IEEE 929, a document that defines unacceptable islanding and a method for evaluating energy sources. The worst expected loads for an islanded inverter are defined in IEEE 929 as being composed of passive resistance, inductance, and capacitance. However, a controversy continues concerning the possibility that a capacitively compensated, single-phase induction motor with a very lightly damped mechanical load having a large rotational inertia would be a significantly more difficult load to shed during an island. This report documents the result of a study that shows such a motor is not a more severe case, simply a special case of the RLC network.

## Table of Contents

Introduction .....	5
Procedure .....	7
Results .....	14
Discussion .....	17
Experimental Verification of Results .....	17
Conclusion .....	21
References .....	22
Appendix A .....	23

## Introduction

Islanding of a grid-connected distributed generation (DG) system, such as a photovoltaic (PV) system, occurs when the DG continues to energize a portion of the utility system after that portion has been disconnected from the main utility voltage source. Consider the system configuration shown in Figure 1. The PV system consists of the PV array and DC-AC converter, or inverter, at the left. The utility voltage source is represented at the far right. There is also a switch that can isolate the utility voltage from the other components shown. The node labeled “Node A” is the point of common coupling between the customer load and the utility system. If the PV system continues to energize the components to the left of the switch after the switch has been opened, then the PV system is islanding. Because islanding represents a potential hazard to personnel and property, applicable codes and standards require that DG systems incorporate methods to prevent it. For example, the IEEE-929-2000 standard, Recommended Practice for Interconnection of Photovoltaic and Utility Systems, requires that a PV system be interfaced to a utility only through an inverter that has been listed as “non-islanding,” and describes the characteristics of a non-islanding inverter [1].

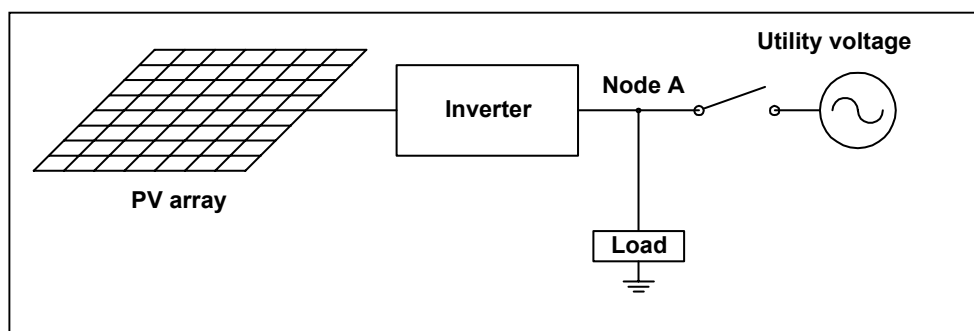


**Figure 1. System configuration for understanding islanding**

In order to verify that an inverter is non-islanding, groups administering listing or certification need a test that can be applied to an inverter that will determine whether it meets the specifications laid out in IEEE-929. Such a test was developed by a team led by Sandia National Laboratories (SNL) in the late 1990s [2]. The ability of an inverter to detect islanding is largely dependent on the electrical load present in the island (see Figure 1). Some loads do not interfere with islanding detection, whereas others make islanding detection extremely difficult. A great deal of theoretical and experimental study was done to determine the types of loads that could be expected to cause the most difficulty [3,4,5]. The rationale was that if a realistic worst-case type of load could be defined, DGs could be tested with that load, and if they detected islanding with the worst-case load they could be expected to reliably detect islanding under real-world conditions. The result of the studies was that the worst-case load appeared to be a parallel  $RLC$  load in which (1) the resonant tank was very large (i.e., large  $C$ , small  $L$ ), and (2) the resonance was very lightly damped (i.e.,  $R$  is large). Such loads may be conveniently described using the quality factor  $Q$  of the parallel  $RLC$  load:

$$Q = R\sqrt{\frac{C}{L}} \quad [1]$$

The worst-case *RLC* load described above corresponds to a load with a high value of  $Q$ , *and* a resonant frequency within the DG's under- and over-frequency trip setpoints. (It is important to note that both conditions are important; an extremely high- $Q$  load with its resonant frequency outside the trip setpoints of the DG will *not* lead to long run-on times.) With such a load, the time between disconnection of the utility and the time at which the PV inverter detects islanding and discontinues operation, known as the run-on time, could be very long, or even indefinitely long. Thus, SNL personnel specified a test using this type of parallel *RLC* load.

As might be expected, further experimentation raised further questions. One particularly troubling question arose repeatedly: Experimenters were inconsistently observing that they could get very long run-on times if, instead of using the worst-case parallel *RLC* load, they used a load containing a capacitively compensated, single-phase induction motor with a very lightly damped mechanical load that had a large rotational inertia [2,6]. The most common realization of this type of load was a bench grinder, a motor driving one or more large stone grinding wheels acting as flywheels.

A proposed explanation for this phenomenon was that the flywheel, whose time constant is several orders of magnitude slower than that of the electrical system, could act as a prime mover during the electrical transient. Its rotational inertia could turn the induction machine as a generator, sending its kinetic energy into the island and maintaining the voltage that causes the PV system to continue operating. However, theory suggested that this was not possible. In order for the single-phase induction machine to act as a generator, assuming the rotational speed to be held constant by the large rotational inertia, it would be necessary for the electrical frequency in the island to change. According to the basic theory described below, under practical conditions, a single-phase induction motor generally cannot reach its generator range of operation without reaching the under-frequency trip setpoint of the PV system, causing it to trip off line.

However, the question remained as to why longer run-on times were being seen with motors than with the *RLC* loads. In fact, this question was sufficiently troubling to some standards-making bodies that they proposed to include motors in the loads used to test non-islanding inverters. This solution presents extreme logistical problems with reproducibility, as it is difficult to make certain all certifying organizations use the "same" motor. Even specifying the "standard" motor for use in the tests would be difficult as there is such a wide range of motor sizes and types in use.

As these difficulties became apparent, SNL initiated a study to determine whether in fact the induction machine represented a worst-case load, and thus whether it was necessary to include motors in test loads. This document describes the results of this study.

## Procedure

As described above, theory suggests that the explanation that the motor is acting as a generator is not possible because of the physics of the induction machine. To understand why this is so, consider the electrical schematic of the single-phase induction machine shown in Figure 2 [7].

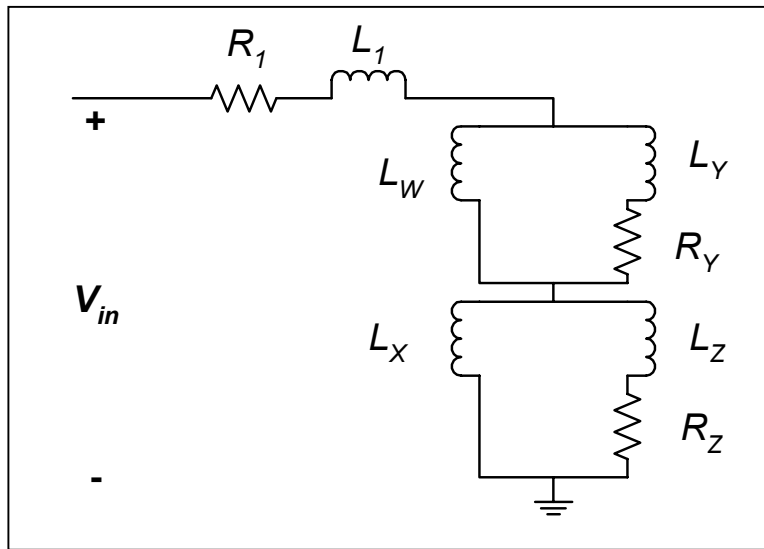


**Figure 2. Schematic of a single-phase induction machine [7]**

The voltage  $V_{in}$  applied to the terminals of the machine is the motor's driving voltage. The various electrical, magnetic, and mechanical mechanisms within the machine may be represented by the combination of inductors and resistors shown. The values of resistors  $R_Y$  and  $R_Z$  are functions of the mechanical load on the machine (and a variety of other factors) through a parameter known as the *slip*. The slip  $S$  is defined as

$$S = \frac{[\text{electrical synchronous frequency}] - [\text{mechanical frequency}]}{[\text{electrical synchronous frequency}]} \quad [2]$$

where the electrical synchronous frequency is proportional to the frequency of the applied voltage  $V_{in}$  (it is the frequency of  $V_{in}$  divided by the number of magnetic pole pairs in the machine), and the mechanical frequency is the rotational frequency of the machine and load (assuming no gears). Note that the slip is always less than 1. Typically, for a single-phase machine under steady-state, 60 Hz operation,  $S$  is on the order of 0.05. The torque produced by the machine is in part a function of the slip, and in this way the steady-state operating value of the slip depends on the mechanical load.

The relationships between  $R_Y$  and  $R_Z$  and the slip are [7]:

$$R_Y = \frac{R}{2S} \quad [3]$$

$$R_Z = \frac{R}{2(2-S)} \quad [4]$$

where  $R$  is a constant for a specific machine. Thus, since  $S$  depends on the electrical and mechanical frequencies, the resistances  $R_Y$  and  $R_Z$  are also functions of the electrical and mechanical frequencies.

In the present case in which the rotational inertia of the load is very large, the mechanical frequency can be considered to be constant over time periods of interest. Thus,  $S$ ,  $R_Y$  and  $R_Z$  depend on electrical frequency only. In order for the machine represented in Figure 2 to enter the generator mode of operation, the resistance  $R_Y$  must become negative, and Equation 3 clearly shows that the only way for this to occur, since  $R$  is positive, is for  $S$  to become negative. According to Equation 2, since the mechanical frequency is (approximately) constant in our case, there must be a decrease in electrical frequency to obtain generation. If we assume 60 Hz electrical excitation and a slip of 0.05, then the frequency at which the slip becomes zero would be 57 Hz, and must drop below that to obtain generation. Since IEEE-929-2000 already requires PV inverters to trip off line if the frequency drops below 59.3 Hz, this condition clearly would be detected by the inverter. This is the reason for the previous statement that theory suggests that the induction machine cannot be causing longer run-on times through generation.

What, then, is the reason for the experimental observation of longer run-on times with induction motors? As mentioned in the Introduction, it is well known now that the larger the value of  $Q$  of an  $RLC$  circuit is (i.e., the larger the energy stored in the resonant circuit is relative to what is dissipated), the longer the run-on times will be, provided that the load's resonant frequency is within the DG's frequency trip setpoints. The inductive energy storage in an induction machine is typically very large (the equivalent value of  $L$  is small), and the value of capacitance  $C$  required to compensate it is large. This means that a motor load can be thought of as a practical way to realize the high- $Q$  " $RLC$ " load already known to be a worst case for islanding detection. (" $RLC$ " is placed in quotes because the motor load is not a parallel  $RLC$  circuit.) In fact, an examination of some of the earlier results [2,6] indicates that when the experimenters compared motor and  $RLC$  loads, the values of capacitance used in the motor load cases were three or more times larger than that used in the  $RLC$  loads. Thus, the postulate proposed here is that in fact the rotating load has little or nothing to do with the extended run-on times observed. Rather, they are caused by the fact that the capacitively compensated motor load conveniently realizes a more severe case of the already known worst-case high- $Q$   $RLC$  load.

To test this theory, the following procedure was adopted. First, computer simulations were used to test "equivalent" motor and  $RLC$  loads. Equivalent loads are

defined as loads that have identical complex impedances; that is, the complex impedances presented to the utility and DG by the equivalent loads will be the same. The computer simulated a utility with its impedance, either an *RLC* or capacitively compensated induction machine load, and a DG (considered herein to be a photovoltaic [PV] system) equipped with the Sandia Frequency Shift (SFS) method of islanding detection. Simulations were run with loads including capacitors closely matched to the resonant value, and the behavior of the PV system was quantified by plotting the frequency of the voltage at Node A in Figure 1. The frequency trajectories of the system with the different loads were compared to determine whether there is a significant difference between the system's behavior with the different loads.

In order to simulate the systems, mathematical models for each were derived. Both systems have the basic configuration shown in Figure 1, but one has a parallel *RLC* load (Figure 3), and the other a capacitively-compensated induction motor load (Figure 4). The PV system was represented as a controlled current source producing the SFS waveform [3,4,8]. The initial chopping fraction (percent of zero time in the current waveform under normal steady-state conditions) was zero, and the chopping fraction gain was set to be 5 %/Hz. The amplitude of the PV output current was selected to exactly balance the required load current. The dynamics of the PV system, particularly the inverter, were not modeled. The impedances  $R_U$  and  $L_U$  represent the utility impedance. It is assumed here that the utility impedance is dominated by the local transformer, and thus values were chosen to match those of a common transformer [9].

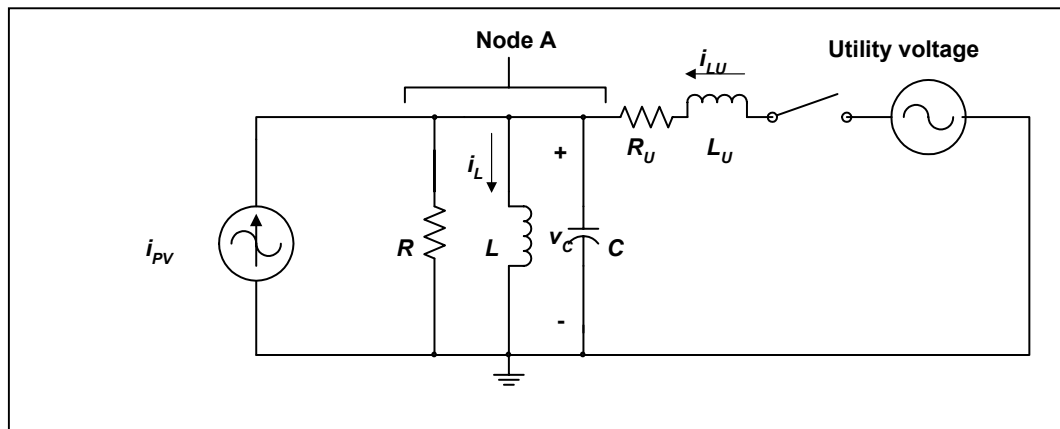


**Figure 3. System configuration with an *RLC* load**

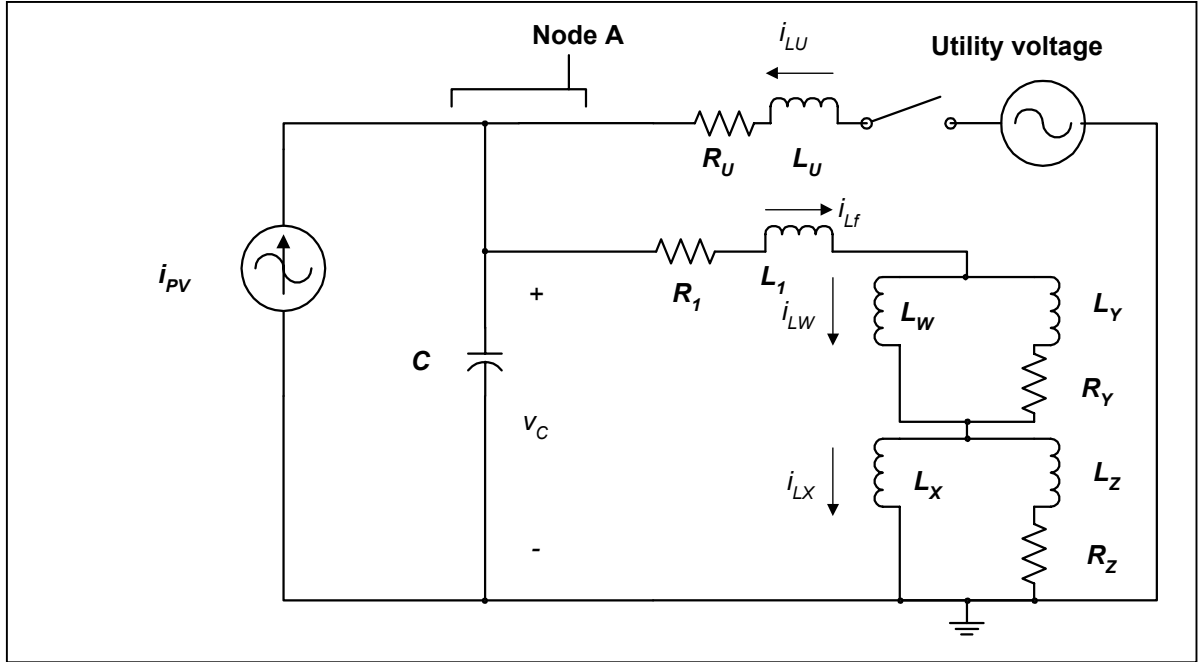


**Figure 4. System configuration with a capacitively-compensated induction motor load**

For each system, state space models were derived. The derivation proceeds as follows. For the system with the  $RLC$  load, the state variables, referring to Figure 3, were chosen to be the load inductor current,  $i_L$ , the load capacitor voltage,  $v_C$  (which is also the Node A voltage), and the utility inductor current,  $i_{LU}$ . The inputs are the PV system current,  $i_{PV}$ , and the utility voltage,  $v_U$ . The state and input vectors are thus defined as

$$X = \begin{bmatrix} i_L \\ v_C \\ i_{LU} \end{bmatrix} \quad [5]$$

$$U = \begin{bmatrix} i_{PV} \\ v_u \end{bmatrix}$$

Most of the mathematical details of the derivations will be omitted here but are available from the author upon request. Using Kirchoff's Laws and the basic I-V relationships of the various components, the state space model for the system with the utility connected is found to be

$$\frac{d}{dt} \begin{bmatrix} i_L \\ v_C \\ i_{LU} \end{bmatrix} = \begin{bmatrix} 0 & \frac{1}{L} & 0 \\ -\frac{1}{C} & -\frac{1}{RC} & \frac{1}{C} \\ 0 & -\frac{1}{L_U} & -\frac{R_U}{L_U} \end{bmatrix} \cdot \begin{bmatrix} i_L \\ v_C \\ i_{LU} \end{bmatrix} + \begin{bmatrix} 0 & 0 \\ \frac{1}{C} & 0 \\ 0 & \frac{1}{L_U} \end{bmatrix} \begin{bmatrix} i_{PV} \\ v_U \end{bmatrix} \quad [6]$$

and the output equation is

$$v_A = \begin{bmatrix} 0 & 1 & 0 \end{bmatrix} \cdot \begin{bmatrix} i_L \\ v_C \\ i_{LU} \end{bmatrix} \quad [7]$$

When the utility is disconnected, the system configuration changes. The new system model is obtained from the one above by eliminating all the terms associated with  $i_{LU}$ ; that is, by eliminating the third row and third column of the system matrix, and the third row and second column of the input matrix. This model was used in the MATLAB math software package to perform the desired simulations.

For the motor load case, referring to Figure 4, the state variable matrix is:

$$X = \begin{bmatrix} v_C \\ i_{L1} \\ i_{LW} \\ i_{LX} \\ i_{LU} \end{bmatrix} \quad [8]$$

Note that  $i_{LY}$  and  $i_{LZ}$  should *not* be selected as state variables because they are not independent; if, for example, we know  $i_{L1}$  and  $i_{LW}$ , then we know  $i_{LY} = i_{L1} - i_{LW}$ , and similarly  $i_{LZ} = i_{L1} - i_{LX}$ . Also, because we are assuming that the motor's rotational speed is approximately constant over the interval of interest, the motor's rotational speed is not included as a state variable, and the motor torque equation is not needed. The input matrix is the same as in the *RLC* load case. As before, it is a relatively simple matter to find equations for the time derivatives of the capacitor voltage and utility inductor current using Kirchhoff's laws and the basic I-V relationships of the components:

$$\frac{dv_c}{dt} = -\frac{1}{C}i_{L1} + \frac{1}{C}i_{LU} + \frac{1}{C}i_{PV} \quad [9]$$

$$\frac{di_{LU}}{dt} = -\frac{1}{L_U}v_c - \frac{R_U}{L_U}i_{LU} + \frac{1}{L_U}v_U \quad [10]$$

Finding equations for the time derivatives of the other three state variables is slightly more complicated. If we use the basic relationships as before, we can find three equations in three unknowns (namely the three desired time derivatives). If Kirchhoff's Voltage Law is applied to a loop containing  $C$ ,  $R_I$ ,  $L_W$ , and  $L_X$ , and also around the two closed  $R$ - $L$  loops in the induction motor model, and the above-noted expressions for  $i_{LY}$  and  $i_{LZ}$  are used, the following equations are obtained.

$$L_1 \frac{di_{L1}}{dt} + L_W \frac{di_{LW}}{dt} + L_X \frac{di_{LX}}{dt} = v_c - i_{L1}R_1 \quad [11]$$

$$[L_W + L_Y] \frac{di_{LW}}{dt} - L_Y \frac{di_{L1}}{dt} = R_Y [i_{L1} - i_{LW}] \quad [12]$$

$$[L_X + L_Z] \frac{di_{LX}}{dt} - L_Z \frac{di_{L1}}{dt} = R_Z [i_{L1} - i_{LX}] \quad [13]$$

We now have a set of five equations in the five unknowns in our system:

$$M_1 \frac{dX}{dt} = M_2 X + M_3 U \quad [14]$$

$$M_1 = \begin{bmatrix} C & 0 & 0 & 0 & 0 \\ 0 & L_1 & L_W & L_X & 0 \\ 0 & -L_Z & 0 & L_X + L_Z & 0 \\ 0 & -L_Y & L_W + L_Y & 0 & 0 \\ 0 & 0 & 0 & 0 & L_U \end{bmatrix}; M_2 = \begin{bmatrix} 0 & -1 & 0 & 0 & 1 \\ 1 & -R_1 & 0 & 0 & 0 \\ 0 & R_Z & 0 & -R_Z & 0 \\ 0 & R_Y & -R_Y & 0 & 0 \\ -1 & 0 & 0 & 0 & -R_U \end{bmatrix}; M_3 = \begin{bmatrix} 1 & 0 \\ 0 & 0 \\ 0 & 0 \\ 0 & 0 \\ 0 & 1 \end{bmatrix}$$

This equation is not in the standard form for state space systems, which is

$$\frac{dX}{dt} = AX + BU$$

However, it can be put into the standard form easily if the matrix  $M_1$  is invertible, which it is in the present case. Thus we premultiply both sides of the equation by  $M_1^{-1}$  and identify

$$A = M_1^{-1}M_2$$

$$B = M_1^{-1}M_3$$

This completes the derivation.

In order to find the capacitor that exactly compensates the motor load to a unity power factor (i.e., such that the imaginary part of the compensated motor's impedance is zero), an expression for the imaginary part of the compensated motor impedance was derived. The impedance of the motor is

$$Z_{motor} = R_1 + j\omega L_1 + \left[ \frac{1}{j\omega L_W} + \frac{1}{R_Y + j\omega L_Y} \right]^{-1} + \left[ \frac{1}{j\omega L_X} + \frac{1}{R_Z + j\omega L_Z} \right]^{-1} \quad [15]$$

$$\equiv x + jy$$

where  $\omega$  is the electrical frequency in radians per second. This complex impedance  $x + jy$  is in parallel with the compensating capacitor impedance:

$$Z_{load} = \frac{1}{j\omega C + 1/Z_{motor}} = \frac{1}{j\omega C + 1/(x + jy)} \quad [16]$$

The imaginary part of  $Z_{load}$  is then isolated and set equal to zero (for a unity power factor load), and solved for  $C = C_{res}$ , the resonant capacitance. After considerable manipulation, the result is

$$C = \frac{y}{\omega(x^2 + y^2)} \equiv C_{res} \quad [17]$$

Once the motor parameters are chosen, the values of  $x$  and  $y$  can be found easily in MATLAB, and the compensating  $C_{res}$  can be calculated using Equation 17.

To find the  $RLC$  load equivalent to the given motor load, the real and imaginary parts of the  $RLC$  load must be equivalent to those of the motor load. First, the value of  $L$  can be calculated because the value of  $C_{res}$  is already known, and

$$L = \frac{1}{\omega^2 C_{res}} \quad [18]$$

The real part of the  $RLC$  load will be determined by  $R$  and must be set equal to the real part of the compensated motor load.

Having derived the needed state-space models, MATLAB programs were written to simulate both system configurations. The motor and *RLC* load parameters used are included in Appendix A at the end of this document. (The reader is encouraged to note that, as previously mentioned, choosing a “typical” set of induction motor parameters is extremely difficult because of the wide range of values possible in practice. The set selected here represents a “reasonable” set from the literature.) Simulations were run with several values of  $C$ , all near to  $C_{res}$  but slightly different so that the frequency behavior can be seen. (If a value exactly equal to  $C_{res}$  is used, there should be practically zero frequency deviation in either case.) Thus, the resonant frequency of the circuit is always within the frequency trip limits of the DG. The  $Q$  factors of the *RLC* loads used here are all  $\approx 2$ , ranging from about 1.800 to 2.006. The DG is modeled as a controllable current source operating at unity power factor. A negative-to-positive zero crossing detector detected the rising zero crossings of the Node A voltage. When such a crossing is detected, the frequency is calculated using the time since the previous zero crossing. The measured frequency is stored for plotting and is also used to dynamically recompute the motor slip using Equation 1.

## **Results**

The results of the simulations are shown in Figure 5. Results are shown for both *RLC* and motor loads for several values of  $C$ , found by multiplying  $C_{res}$  by 0.975, 0.99, 1.01, and 1.025. (If  $C$  is set exactly equal to  $C_{res}$ , there is no measurable frequency deviation for either load, but this case does not test the theory.) The motor's starting (steady-state) slip was set to 5%, corresponding to a speed of 1710 rpm.

The utility disconnects at cycle 75.4, a number selected arbitrarily. The choice of the moment of disconnection does make a small difference in run-on times, with run-on lasting slightly longer if the utility happens to be cut off at or very near a rising zero crossing. This difference is not significant. A relatively long time was allowed between the start of the simulation and the utility disconnect time to allow confidence that transient effects are not affecting the results. (The transients were largely eliminated in the first place by careful selection of initial conditions. The motor load cases do exhibit a transient, visible on the plot, but it decays within five line cycles.) Note that the frequency trajectories for equivalent *RLC* and motor loads are practically identical. In fact, according to the theory, the motor load actually produces a slightly larger frequency deviation than does the *RLC*. This small difference is due to the dependence of the motor's equivalent resistance on electrical frequency.

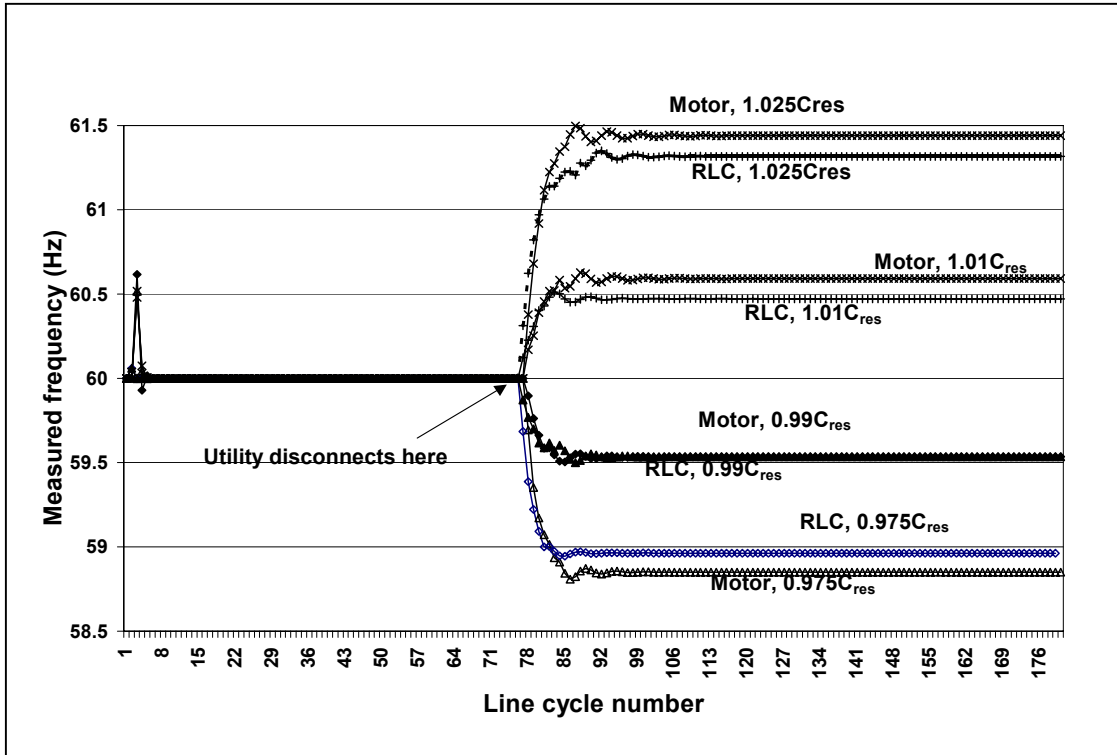


**Figure 5. Simulated Plots of the frequency of the Node A voltage for several load cases**

Not all induction machines operate with a steady-state slip of 5%, and a smaller steady-state slip could lead to different conditions. Thus, a second set of simulations was run with a starting slip of 1.67%, corresponding to a speed of 1770 rpm. The results of two of these simulations with two different values of compensating capacitance are shown in Figure 6.

For the cases illustrated by Curves 2) and 4) in which the compensating capacitance is 1.01 times the resonant capacitance value, the frequency trajectories are extremely similar. There are small differences in the transient behavior immediately after the utility is disconnected, and very slight differences in final steady-state frequency. Both of these are attributable to the small difference in the value of the resistive part of the motor's electrical load, which is caused by the change in slip (see Equations 2 and 3). Thus, in these cases, the change in initial slip did not make a significant difference in the system's behavior.

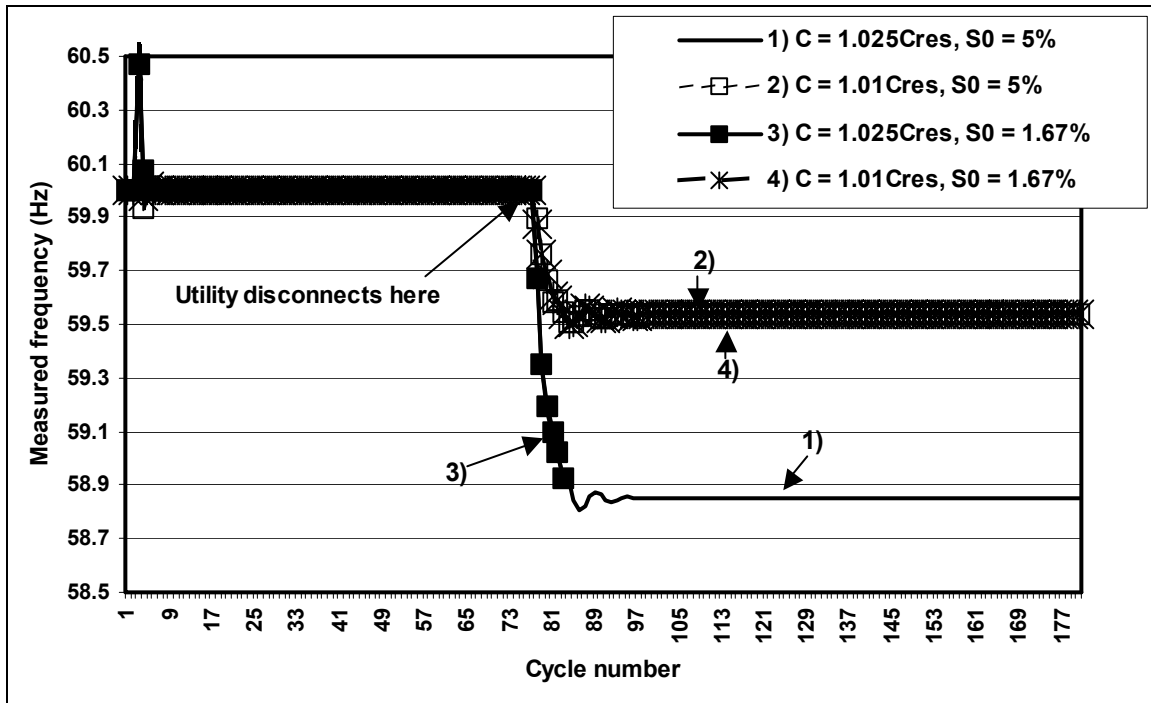


**Figure 6. Simulated Plots of the frequency of the Node A voltage for the induction motor load with starting slip values ( $S_0$ ) of 5% and 1.67%**

A different scenario is presented by Curves 1) and 3) in Figure 6 for compensating capacitance values of  $C_{res} \times 1.025$ . In this case, there is a rapid drop in the Node A frequency immediately after utility cutoff. For the initial slip of 5%, the system reached a new steady-state frequency, just as it did with the other capacitance values. However, for the initial slip of 1.67%, the reader will note that the trace ends in cycle number 89. At that point, the motor entered the generation mode of operation. Almost immediately thereafter, there was a large voltage transien Node A. This happened because induction generators do not have the capability of controlling their terminal voltage [10]. Induction machines do not have controllable field circuits because their internal magnetic fields cannot be regulated to create a well-controlled terminal voltage. In practice, when an induction generator is used (i.e. as a wind turbine), the external power system must regulate the generator's terminal voltage. However, in the present case, the DG, acting as a current source, does not regulate the Node A voltage, and thus the induction generator's terminal voltage fluctuates widely upon utility disconnection. This fluctuation in the Node A voltage always led to an overvoltage trip in our simulations, leading to an immediate system shutdown and very short run times. This is the case shown in Figure 6; the frequency trajectory for  $C = 1.025 \times C_{res}$ ,  $S_0 = 1.67\%$  actually stops at Cycle Number 90. It should be noted that if the DG in the island does have voltage regulation capability, then this result could be different. The reader should also remain aware that, as seen in Figure 6, the frequency of the Node A voltage was below 59 Hz and was thus well outside the allowed window before the generation mode was observed.

## **Discussion**

The simulations suggest that the explanation proposed here is correct; the extended run-on times observed for single-phase induction motor loads in the past are caused by the fact that the motor load conveniently represents an analog to the already-known worst case load for islanding prevention, the high- $Q$  parallel  $RLC$  circuit with resonant frequency very near the line frequency. Furthermore, it appears that if the induction machine were to enter the generation mode, the possibility of islanding would actually be reduced due to the lack of voltage regulation in the island, unless the DG in use has voltage regulation capability. It must be borne in mind that this simulation does neglect the variation of motor rotational speed with changing electrical frequency. After a time, the rotational speed will change slightly, reaching a new value determined by the required load torque and the motor characteristics. However, over the frequency range shown here, this change would be very small and probably too small to affect the basic result.

A brief discussion of the extension of these results to larger DGs feeding three-phase induction machines is in order at this point. The development here has concentrated on single-phase machines because these are the type used in virtually all of the experiments to date. However, three-phase machines have an equivalent circuit that is similar to that of the single-phase machine in that there is a resistance value that depends on slip, and the machine cannot enter the generation mode unless the slip becomes negative [7, 11]. Therefore, the basic behavior of the three-phase system, in terms of islanding prevention, should not be significantly different than that of the single-phase system presented here. In other words, the three-phase motor may also be sufficiently modeled by a three-phase  $RLC$  load. One potential difference between the three-phase and single-phase cases is that three-phase motors, in general, tend to operate at lower slip values. Thus, the case in which the generator mode is seen could be more prevalent for three-phase machines.

## **Experimental Verification of Results**

Simulation cannot replace experimentation. Therefore, the following experiment was performed at SNL to verify the simulation results. The DG, a PV system, used the SFS islanding prevention method for maximum compatibility with the simulation results. Note, however, that this was not necessary, as the fundamental conclusion reached above is independent of the islanding prevention method used.

### **Part I**

- (1) The first load to be tested was a 1/2-horsepower bench grinder driven by a single-phase induction machine. The grinder was not mechanically loaded (i.e. the grinding wheels were allowed to spin freely). The complex impedance of the motor was determined by applying 60 Hz power to the motor, allowing it to come to steady state, and using a power meter to characterize the current drawn by the

motor. The results of these measurements, without capacitive compensation, are given in Table 1. The current waveform drawn by the uncompensated motor is shown in Figure 7. Note that there is a small amount of distortion (almost 6% THD, as given in Table 1).

- (2) The motor was then capacitively compensated to nearly unity power factor at 60 Hz, and the characterization measurements were repeated on the compensated motor. The results of these measurements are given in Table 2. The level of distortion in the current was higher in this case, as indicated by the THD measurements in Table 2 and the plot of the compensated motor current in Figure 8. (This is important because it has been previously shown [3] that nonlinearities in local loads should lead to shorter run-on times.)
- (3) The ratio of DG input power to load power,  $P_{gen}/P_{load}$ , was set equal to one.
- (4) Multiple tests were conducted, and the frequency trajectory of the Node A voltage was recorded each time. In some of the trials, the size of the capacitor was set slightly larger than the resonant value, so that the capacitor was supplying slightly more reactive power (VARs) than the load required. Past experience has shown this to lead to slightly longer run-on times, probably because of a slight time delay between the DG's output current waveform and the Node A voltage which is compensated by the slightly larger capacitance.

**Table 1. ½ hp Grinder Load (uncompensated)**

Quantity	Value	Quantity	Voltage	Current
Frequency	59.96	RMS	121.47	3.5
KW	0.18	Peak	172.96	4.98
KVA	0.43	DC Offset	-0.01	-0.03
KVAR	0.39	Crest	1.42	1.42
Peak KW	0.64	THD Rms	1.58	5.71
Phase	66° lag	THD Fund	1.58	5.72
Total PF	0.41	HRMS	1.92	0.2
DPF	0.41	KFactor		1.09

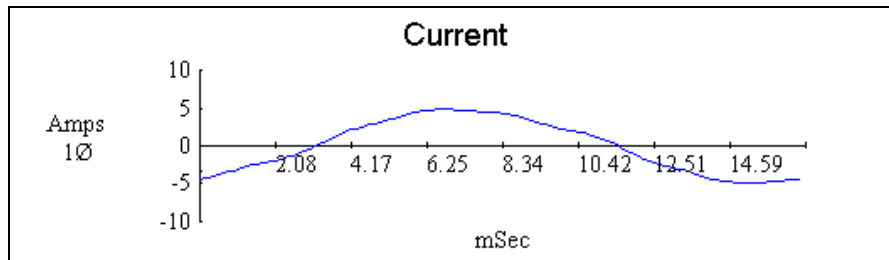


**Figure 7. Grinder current waveform**

**Table 2. ½ hp Grinder Load (compensated)**

Quantity	Value	Quantity	Voltage	Current
Frequency	59.96	RMS	120.57	1.42
Watts	169	Peak	172.3	2.09
VA	171	DC Offset	-0.02	-0.03
Vars	1	Crest	1.43	1.47
Peak W	359	THD Rms	1.27	15.5
Phase	1° lag	THD Fund	1.27	15.69
Total PF	0.99	HRMS	1.53	0.22
DPF	1	KFactor	2.22	

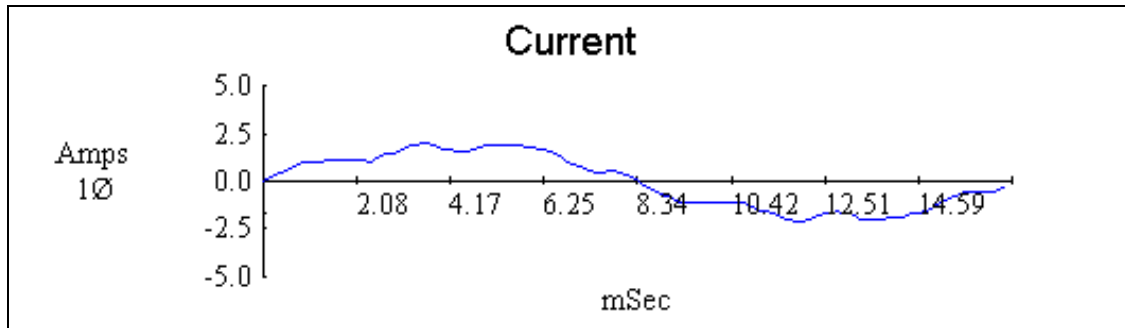


**Figure 8. Compensated grinder current waveform**

## Part II

- (5) Next, an *RLC* load with the same complex impedance as the motor load tested in Part I was set up.
- (6) The  $P_{gen}/P_{load}$  ratio was equal to one, and multiple trials were conducted with the frequency trajectory recorded each time.

The experimental results are given in Figures 9 and 10 below. Figure 9 shows the trajectories of the frequency of the Node A voltage for the compensated motor load. Results are shown for eleven trials, ten with the motor compensated to unity power factor, and one with a slightly larger capacitance (labeled as "+33 Capacitive Vars" in the figure). Past experience with the particular inverter being used in these tests has suggested that a slightly capacitive load gives somewhat longer run-on times. This is thought to be caused by a small delay between the inverter's terminal voltage and its output current (in other words, a small frequency bias) produced by delays in the microcontroller-based control circuits and the dynamics of the inverter, among other things. The trigger (point of disconnection of the utility) is shown as a heavy black line. In almost all cases, the PV system's inverter ceases operation approximately 0.8 seconds after the utility disconnection. In the larger capacitor case, the run-on time is slightly

longer. After the DG stops powering the island, there is a long, slow decay in the frequency as the induction machine slows down. This is consistent with the simulation results, and also with prior experience. Previous experiments [6] showed that if power is removed from a bench grinder operating at rated speed and no mechanical load, a slowly decaying voltage can be detected at its terminals for several tens of seconds after power is cut off, as long as the capacitor is still connected. This type of self-excitation is well known. This effect is visible in Figure 9; after the inverter stops supplying power, the motor slowly runs down, and does in fact enter the generation mode once the frequency has declined sufficiently. In other words, the induction machine does enter the generator mode for a few seconds, but *only after the DG has already stopped*. It should be noted that if care is not taken to measure the point at which the inverter actually ceases operation, it would be possible for an experimenter to mistakenly measure a run-on because of the motor's generator action after inverter shutdown.

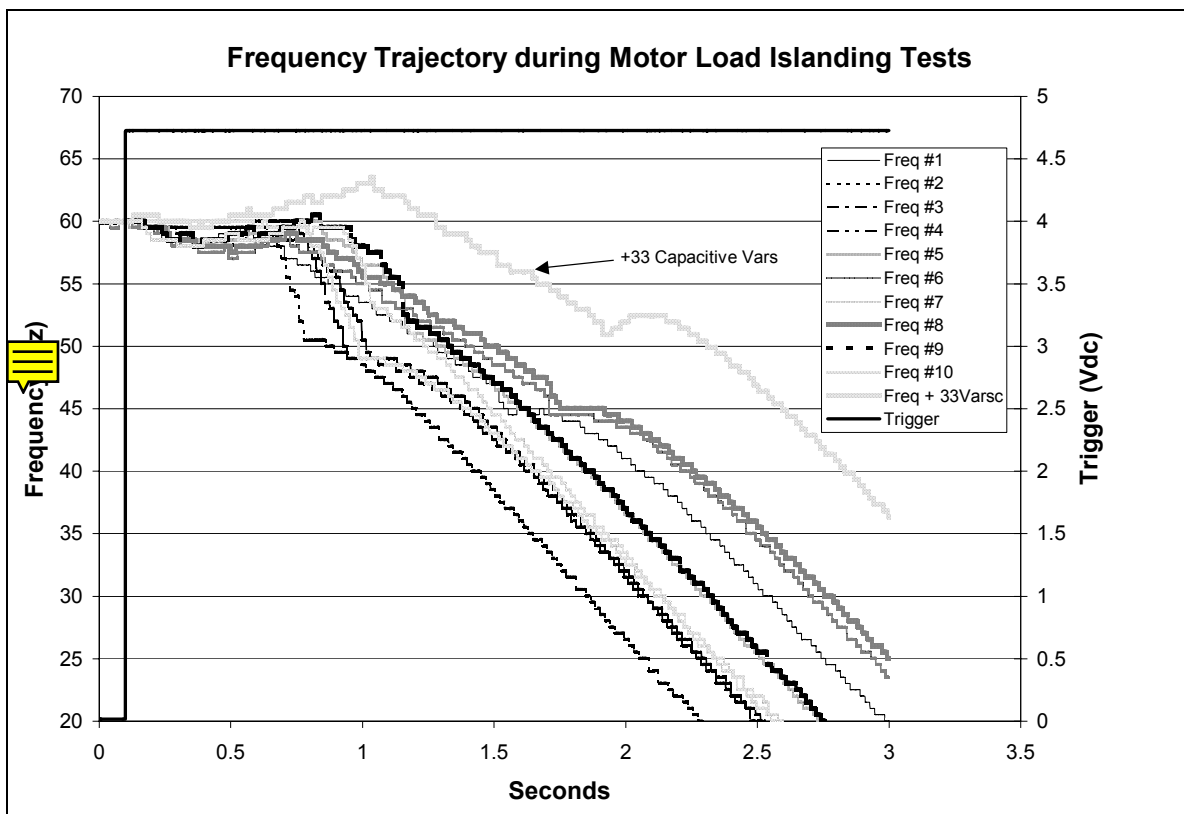


**Figure 9. Trajectories of the Node A voltage frequency for eleven trials. The load is the compensated induction motor load with the flywheel (bench grinder). In all trials, the inverter ceases operation at around 0.8 seconds.**

Figure 10 shows the results for the equivalent  $RLC$  load. Eleven trials are included here as well, ten with a unity power factor load and one with the slightly larger capacitor (again labeled "+33 Capacitive Vars"). The run-on times vary somewhat in these trials, but on average they are longer than for the motor load case, and in fact two

cases, including the +33 Capacitive Vars case, run on for over three seconds because these loads lie within the inverter's NDZ. Note that no such long run-ons were observed with the motor load. (It should be noted that in all cases the inverter eventually did stop on its own, without operator intervention; there were no indefinite run-ons.)

The experimental results indicate that the average run-on times found with the motor load are very similar to, but shorter than, those obtained with the resonant *RLC* load. Thus, the experiment verifies the modeling results.

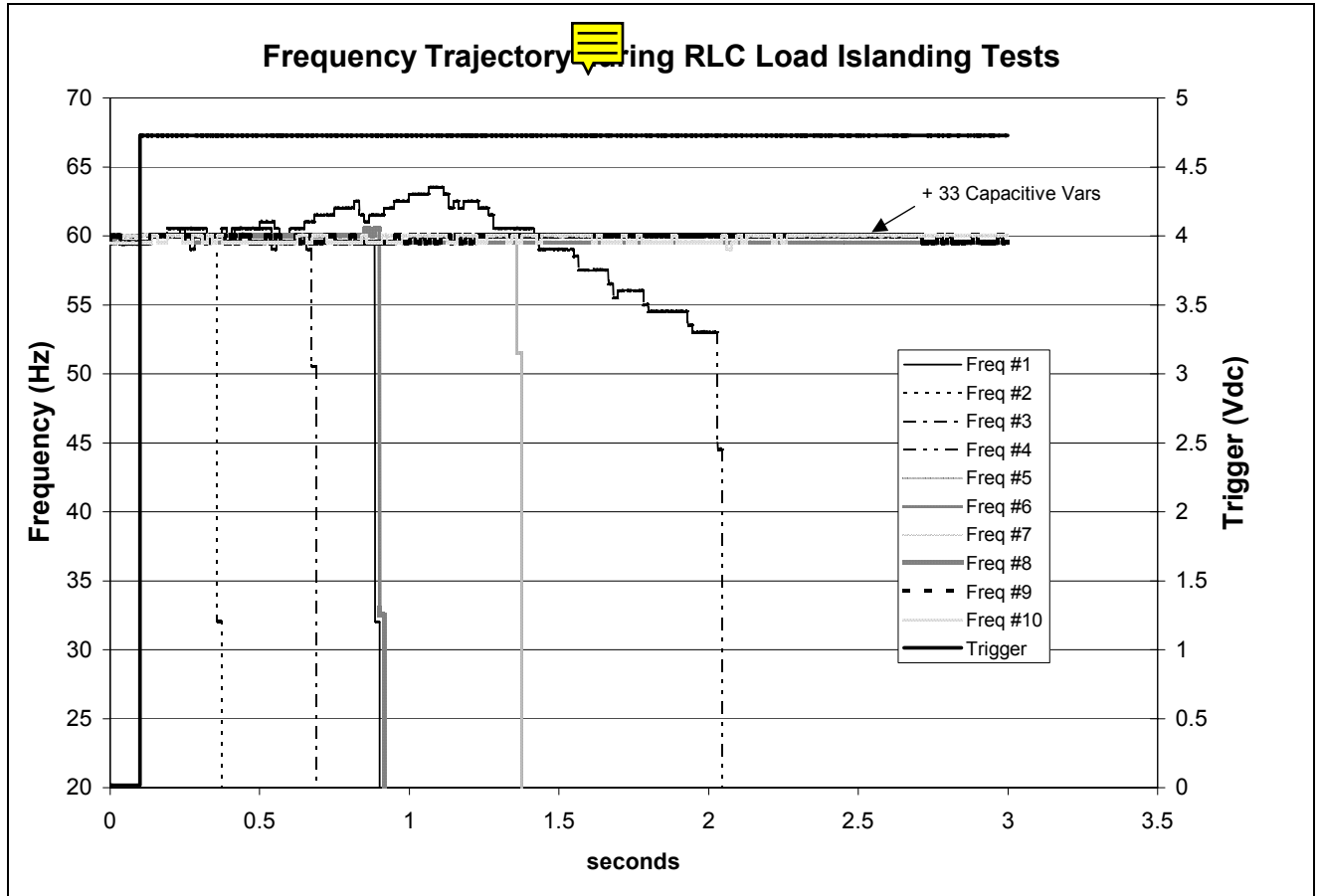


**Figure 10. Trajectories of the Node A voltage frequency for eleven trials. The load is the *RLC* load. Run-on times varied, but in most cases run-on times were longer for this load than for the motor, and the average run-on time is longer for this case. Note that for the larger capacitor case, the run-on time exceeded 3 seconds. (The inverter eventually did stop without operator intervention; it did not run on indefinitely.)**

**Conclusion**

Based on both the simulation and experimental results, it is possible to conclude that induction motors do not represent a worse case load than the previously described

worst-case  $RLC$  load (high  $Q$ , and a resonant frequency within the trip setpoints of the DG). In fact, induction machines can be thought of as implementing a special case of that worst-case  $RLC$  load. It can also be concluded that the Sandia inverter test using the parallel  $RLC$  load does adequately test that inverters will not island, even in the presence of induction machines. It is not necessary to augment the test with induction machines.

### **Suggested future work**

Two directions for future work are suggested by this study. First, it would be instructive to repeat this analysis using a full transient electromagnetic model for the single-phase induction machine, to verify the appropriateness of the simplified model used here. Second, this study did not consider three phase machines in detail, particularly such issues as phase and winding interactions and unbalanced conditions. A treatment of three phase machines would be a useful extension of this study.

### **References**

- [1] IEEE Standard IEEE-929, *Recommended Practice for Utility Interface of Photovoltaic (PV) Systems*, 1999.
- [2] J. Stevens, R. Bonn, J. Ginn, S. Gonzalez, and G. Kern, *Development and Testing of an Approach to Anti-Islanding in Utility-Interconnected Photovoltaic Systems*, Sandia National Laboratories Report, SAND2000-1939, August 2000.
- [3] M. Ropp, Design Issues for Grid-Connected Photovoltaic Systems, PhD dissertation, Georgia Institute of Technology, Atlanta, GA, December 1998.
- [4] M. Ropp, M. Begovic, A. Rohatgi, "Prevention of islanding in grid-connected photovoltaic systems," *Progress in Photovoltaics* 7, 1999, p. 39-59.
- [5] G. Kern, "The physical origins of islanding in dispersed generation systems," draft copy, Ascension Technologies, October 26 1997.
- [6] G. Kern, "Status Report #6, Sandia Anti-Islanding Investigation," contract report to Sandia National Laboratories, May 27, 1998.
- [7] M. Sarma, Electric Machines, 2<sup>nd</sup> ed., pub. West Publishing Co. 1994.
- [8] M. Ropp, M. Begovic, A. Rohatgi, G. Kern, R. Bonn, S. Gonzalez, "Determining the relative effectiveness of islanding detection methods using phase criteria and nondetection zones," *IEEE Transactions on Energy Conversion* 15 (3), September 2000, p. 290-296.
- [9] Parameters of a standard 50-kVA 7620 V – 240 V transformer supplied by Howard Industries, Laurel, MS.
- [10] S. J. Chapman, Electric Machinery Fundamentals, 3<sup>rd</sup> ed., pub. WCB McGraw-Hill, 1998.
- [11] B. Amin, Induction Motors: Analysis and Torque Control, 2<sup>nd</sup> ed., pub. B. Amin 2001.



## Appendix A

### Motor and RLC Load Parameters Used in this Work

The motor parameters used here were taken from page 330 of Reference 7. These parameters were found to be “typical” of single-phase induction machines, but it should be noted that the possible values for these parameters vary widely for actual machines.

For the motor:

$$R_1 = 10 \Omega$$

$$L_1 = 33.16 \text{ mH}$$

$$L_m = L_1$$

$$L_w = L_x = L_y = L_z = 0.5 * L_m$$

$$R_2 = 11.5 \Omega$$

Motor speed before utility disconnection = 1710 rpm (179.1 rad/sec), corresponding to a steady-state slip of 5%

$$C_{res} = C_{comp} = 96.325 \mu\text{F}$$

For the parallel *RLC* load:

$$R = 54.92 \Omega$$

$$L = 73.0 \text{ mH}$$

## Distribution List

